THE MECHANICS OF INTERFACE FRACTURE IN LAYERED COMPOSITE MATERIALS: (5) THIN FILM SPALLATION DRIVEN BY POCKETS OF ENERGY CONCENTRATION – MICROSCOPIC INTERFACE FRACTURE

Bin Wang[1], Christopher M. Harvey[1] and Simon S. Wang[1, 2]

[1] Department of Aeronautical and Automotive Engineering, Loughborough University, Loughborough, Leicestershire LE11 3TU, United Kingdom
E-mails: b.wang2@lboro.ac.uk, c.m.harvey@lboro.ac.uk, s.wang@lboro.ac.uk

[2] School of Mechanical and Equipment Engineering,
Hebei University of Engineering, Handan, China

Keywords: Delamination, Pockets of energy concentration, Thermal residual stress, Spallation

ABSTRACT

A hypothesis is made that delamination can be driven by pockets of energy concentration (PECs) in the form of pockets of tensile stress and shear stress on and around the interface between a thin film and a thick substrate, where PECs can be caused by thermal, electrochemical or other processes. Based on this hypothesis, three analytical mechanical models are developed to predict several aspects of thin-film spallation failure including nucleation, stable and unstable growth, size of spallation and final kinking off. The predictions from the developed models are compared against experimental results and excellent agreement is observed.

1 INTRODUCTION

Thin solid films are found in many different applications fulfilling various roles such as confinement of electric charge in integrated electronic circuits, thermal insulation in thermal barrier coatings (TBCs), and protection against corrosion, friction and wear in surface coatings. Although thin films are not usually expected to have a primary load-carrying capability, they often experience residual stresses due to the fabrication process and/or working conditions. Residual stresses are a major cause of film cracks and debonding. Buckling-driven delamination is a typical example of film failure under in-plane compressive residual stress, which has been extensively studied in the last few decades. However, the experimental studies [1, 2] reveal a completely new failure behaviour of thin layer materials. A hypothesis is proposed in the present work to explain this behaviour. According to this hypothesis, delamination can be driven by PECs in the form of pockets of tensile stress and shear stress, with the former being dominant on and around the interface between a thin film and a thick substrate, where PECs can be caused by a number of different processes, including thermal cooling, chemical reactions and etc. Based on this hypothesis, circular-edged spallations are considered. Three mechanical models are established using partition theories for mixed-mode fracture based on classical plate theory, first-order shear-deformable plate theory and full 2D elasticity.

2 THEORY [3, 4]

Fig. 1 shows a circular separation bubble of radius R_B of thin layer material of thickness h with the subscript B representing the edge of the bubble. The thin layer material is under in-plane biaxial compressive stresses σ_0. The bubble shape is assumed to be radially sinusoidal and axisymmetric and represented by

$$w(r)=\frac{A}{2}\left[1+\cos\left(\frac{\pi r}{R_B}\right)\right] \tag{1}$$

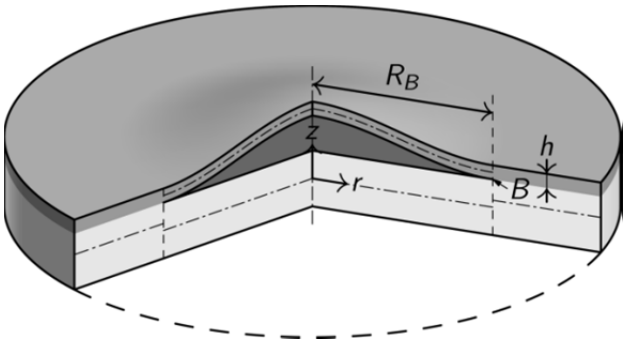

Figure 1: A circular separation bubble of radius R_B .

with w representing the upward deflection and A the amplitude or the maximum separation. A clamped edge condition at $r = R_B$ is assumed because the thickness ratio between the thin layer and substrate is very small. The bubble energy is defined and calculated as

$$U_a = U - U_0 = \pi R_B^2 h \sigma_0 \left\{ \frac{1}{2\bar{\varepsilon}_0} \left(\varepsilon_r^R\right)^2 + \left[\frac{\pi^2}{12\bar{\varepsilon}_0} \left(\frac{h}{R_B} \right)^2 - 1 \right] \varepsilon_r^R + \frac{1}{\varphi_0} \right\} \tag{2}$$

in which U is the total energy in the bubble including the bending strain energy, in-plane strain energy and the interface fracture energy, and U_0 is the residual in-plane strain energy. $\bar{\varepsilon}_0 = \sigma_0(1-\nu^2)/E$ and $\varphi_0 = h\sigma_0/G_c$ where E and ν are the Young's modulus and the Poison's ratio respectively of the thin layer material, and G_c is the interface fracture toughness. It can be shown that U_a is always positive and monotonically increases with respect to the relaxation strain ε_r^R or the bubble amplitude A when $\left(R_B/h\right)^2 < \pi^2/\left(12\bar{\varepsilon}_0\right)$. In this work, U_a is called 'bubble energy'. It comes from the PEC energy formed in the form of pockets of tensile stress and shear stress, with the former being dominant on and around the interface between a thin layer material and the thick substrate. The PECs can be caused by a number of different processes including thermal cooling, chemical reactions and etc. When the PEC energy is able to provide the bubble energy U_a for nucleation, nucleation of a separation bubble will occur. It is expected that the bubble energy U_a governs the growth behavior of a bubble. By using the mixed mode partition theories [5-11] and a linear failure criterion, the bubble energy at bubble growth is obtained.

$$\left(U_a\right)_{GR} = \pi R_B^2 G_c \left\{ \frac{3}{2} + \frac{6\bar{\varepsilon}_0}{\pi^2} \left(\frac{R_B}{h} \right)^2 \left[\frac{3}{\pi^2 \varphi_0} \left(\frac{R_B}{h} \right)^2 - 1 \right] \right\} \tag{3}$$

The first term in Eq. (3) is the sum of the bending strain energy and surface energy while the rest is the relaxed in-plane strain energy, which is negligible if R_B is small. The first term is therefore regarded as the nucleation energy, that is, $\left(U_a\right)_{NU} = 1.5\pi R_B^2 G_c$ where R_B is very small. It is seen that one third of the nucleation energy is used to bend the separation outwards after nucleating the interface separation using two thirds of its energy. When the PEC is able to provide the bubble energy $\left(U_a\right)_{GR}$, it will drive the nucleation and growth of a separation bubble. Two scenarios can occur: One scenario is slow and stable growth which occurs when R_B is smaller than the critical buckling characteristic length. The other is unstable growth when R_B reaches the critical value of the buckling characteristic length. The stable bubble then becomes an unstable buckle. The initiation of unstable growth is found at

$$\left(\frac{R_B}{h}\right)^2_{UG} = \frac{\pi^2\varphi_0}{12}\left[1-\left(1-\frac{\alpha^2}{\Omega}\right)^{1/2}\right] \tag{4}$$

with the subscript UG denoting the initiation of unstable growth and $\alpha = 0.936$, and

$$\Omega = \frac{1}{2}\bar{\varepsilon}_0\varphi_0 = \frac{h\sigma_0{}^2}{2\bar{E}G_c} \tag{5}$$

Ω is the ratio between the plain strain energy density and interface fracture toughness. It will be seen later Ω plays key role for the mechanical behaviour of the bubble. There is no unstable growth when $\Omega < \alpha^2$. Expansion of the expression in the square bracket in Eq. (4) for $\Omega >> \alpha^2$, leads to

$$\left(\frac{R_B}{h}\right)^2_{UG} = \frac{(\alpha\pi)^2}{12\bar{\varepsilon}_0} \tag{6}$$

By differentiating $(U_a)_{GR}$ in Eq. (3) with respect to R_B/h, its maximum is found to occur at

$$\left(\frac{R_B}{h}\right)^2_{MU} = \frac{\pi^2\varphi_0}{9}\left[1-\left(1-\frac{9}{8\Omega}\right)^{1/2}\right] \tag{7}$$

with the subscript MU denoting the maximum. When $\Omega < 9/8$ there is no solution. Expansion of the expression in the square bracket in Eq. (7) for $\Omega >> 9/8$, leads to

$$\left(\frac{R_B}{h}\right)^2_{MU} = \frac{\pi^2}{8\bar{\varepsilon}_0} \tag{8}$$

Note that $(R_B)_{MU}$ in Eq. (8) is approximately equal to the critical buckling radius of a circular bubble with a clamped edge condition. Substituting Eq. (8) into Eq. (3) gives the bubble energy when $\Omega >> 9/8$ as

$$(U_a)_{MU} = \pi R_B^2 G_c\left(\frac{3}{4}+\frac{9}{64\Omega}\right) \approx \frac{3}{4}\pi R_B^2 G_c = \frac{3\pi^3 h^2 G_c}{32\bar{\varepsilon}_0} \tag{9}$$

More importantly, $(U_a)_{GR}$ becomes zero at

$$\left(\frac{R_B}{h}\right)^2_{SP} = \frac{\pi^2\varphi_0}{6}\left\{1-\left[1-\frac{3}{2\Omega}\right]^{1/2}\right\} \tag{10}$$

When $\Omega < 3/2$ there is no solution. Expansion of the expression in the square bracket in Eq. (10) for $\Omega >> 3/2$, leads to

$$\left(\frac{R_B}{h}\right)^2_{SP} = \frac{\pi^2}{4\bar{\varepsilon}_0} \tag{11}$$

At this moment if the kinetic energy due to fast unstable growth of the buckle is large enough to break the film at its edge, the buckle spalls. The subscript SP in the equations above denotes spallation. The

final kink-off angle β can be determined as

$$\beta = \arcsin\left(\frac{32}{3\pi}\frac{G_{cf}}{G_c}\left(\bar{\varepsilon}_0\right)^{1/2}\right) \tag{12}$$

where G_{cf} is the fracture toughness of the thin layer material.

Now, it is worth noting that the above development applies to all the three fracture mode partition theories, i.e. the classical, shear deformable plate [5-9] and 2D elasticity [10, 11] partition theories. However, the interface fracture toughness G_c should be, respectively for the three partition theories,

$$G_c = G_{Ic} \tag{13}$$

$$G_c = \frac{4\psi}{3+\psi}G_{Ic} \tag{14}$$

and

$$G_c = \frac{\psi}{0.3773 + 0.6227\psi}G_{Ic} \tag{15}$$

where G_{Ic} is critical mode I ERR and $G_{IIc} = \psi G_{Ic}$. In the next section, predictions from the theory are compared against experimental observations from Refs. 1 and 2.

3 EXPERIMENTAL ASSESSMENTS

Tolpygo and Clarke [1, 2] presented an excellent experimental study on the room temperature circular spallation of α-alumina films grown by oxidation on Fe-Cr-Al alloy. The theory in Section 2 is applied to predict spallation behaviour [1, 2]. The material properties of the oxide film are taken from Refs. 1 and 2 and are as follows: The Young's modulus of the oxide film is $E = 400\,\text{GPa}$ and the Poisson's ratio is $\nu = 0.25$. The mode I critical ERR of the interface is $G_{Ic} = 8.6\,\text{N/m}$ and the critical mode I ERR of the oxide film is $G_{cf} = 20\,\text{N/m}$. The ratio $\psi = G_{IIc}/G_{Ic} = 5$ is used, which is considered by the authors to be a representative value. First, Eq. (6) is used to predict the initiation of unstable growth, and Eq. (11) is used to predict the size of spallation. The solid dots in Fig. 2 represent a series of measurements of the size of individual separations as a function of time at room temperature. The time of 0 min corresponds to the moment when the specimen was placed under the microscope and its temperature was close to ambient. Fig. 2a shows data from four different separation bubbles on a single specimen after isothermal oxidation for 25 h at 1200°C and cooling at 20°C min^{-1}. The bubbles were successively monitored using optical microscopy. All of the bubbles grew at a constant compressive stress of $\sigma_0 = 4.46 \pm 0.4\,\text{GPa}$, which was measured in the adherent oxide far away from the separations. The whole process includes nucleation, stable growth, unstable growth, and final spallation. The nucleation of separation bubbles was not recorded due to the difficulty of making timely observations of nucleating bubbles using this monitoring technique. Stable growth, however, with a radius far smaller than the critical buckling value, was readily observed. At a certain critical radius, which is again far smaller than the critical buckling radius, unstable growth abruptly occurs and final spallation takes place. It is pertinent that all four separations start unstable growth at approximately the same radius, and then all eventually spall off also at approximately the same radius. Two specimens with thicker oxide layers were produced with 50 h and 100 h of oxidation and are shown in Figs. 2b and c respectively. The growth behaviors of two separation bubbles are shown in Fig. 2b. Again, the two separations start unstable growth at approximately the same radius, and then both eventually spall off also at approximately the same radius. Fig. 2c shows the growth behavior of one separation bubble.

The horizontal lines in Figs. 2a–c represent the predictions from Eq. (6) for the initiation of unstable growth and Eq. (11) for final spallation. It is very impressive to see that the predictions from Eqs. (6) and (11) have

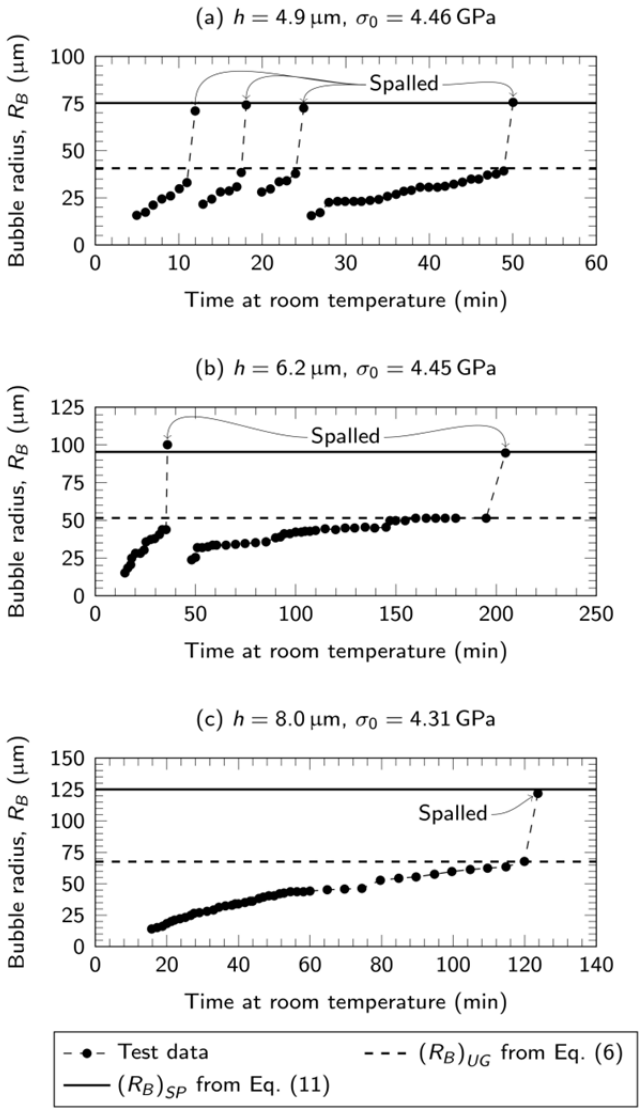

Figure 2: Separation bubble radius versus time at room temperature for three different samples [2].

Excellent agreement with the test results. It is worth noting that Eqs. (6) and (11) are common to all three mechanical models (based on the classical plate, first-order shear-deformable plate and 2D elasticity partition theories) as long as the value of the parameter Ω meets the requirements of Eqs. (6) and (11).

Next, comparisons are made between measurements of the kink-off angle and predictions from Eq. (12). The critical mode I ERR of the oxide film is $G_{cf} = 20\,\mathrm{N/m}$. For Fig. 2a, the value of $h/\tan(\beta) = 9.10\,\mu m$ was measured approximately from Fig. 3 in Ref. [2], which is a similar case. The classical, shear deformable plate and 2D elasticity partition theories give $h/\tan(\beta) = 3.8\,\mu m$, $15.0\,\mu m$, $7.5\,\mu m$, respectively. No test value for Fig. 2b was found in Tolpygo and Clarke's studies [1, 2]. For Fig. 2c, $h/\tan(\beta) = 13.46\,\mu m$ was measured approximately from Fig. 5 in Ref. (2), which is a similar case. The classical, shear deformable plate and 2D elasticity partition theories give $h/\tan(\beta) = 6.1\,\mu m$, $23.9\,\mu m$, $12.0\,\mu m$, respectively. The averages of the measurements of the

four diameters at 0°, 90° and ±45° were used to obtain the test values. It is seen that the 2D elasticity model gives good predictions but the other two models do not.

It can be concluded at this point that the 2D elasticity model predicts the whole delamination process very well, including the initiation of unstable growth, size of spallation and kink-off angle. The other two models, however, only give good predictions of the initiation of unstable growth and the size of spallation.

4 CONCLUSIONS

PECs can be formed by pockets of tensile stress and shear stress on and around the interface between a thin film and a thick substrate, which can be caused by a number of different processes, including thermal effects, chemical effects and etc. PECs can cause interface spallation failure of thin films. Theory has been developed to predict several aspects of thin-film spallation failure by using partition theories for mixed-mode fracture based on classical plate theory, first-order shear-deformable plate theory [5-9] and full 2D elasticity [10, 11]. The three models all give accurate predictions of the initiation of unstable growth of separation bubbles and the size of spallation. The 2D elasticity model also gives accurate predictions of the final kink-off size but the classical plate and first-order shear-deformable plate models are unable to. The nucleation and stable growth of a separation bubble are solely driven by the bubble energy but unstable growth is driven by both bubble energy and buckling. Final kinking off is controlled by the toughness of the interface and the film and the maximum bubble energy. The 2D elasticity partition theory governs the microscopic brittle interface fracture instead of the classical partition theory which governs the macroscopic brittle interface fracture. The present mechanical models reveal a new failure mechanism of thin layer materials under compressive residual stress and will be particularly useful to study the spallation failure of thermal barrier coating material systems.

REFERENCES

[1] V.K. Tolpygo and D.R. Clarke, Spalling failure of α-alumina films grown by oxidation. I. Dependence on cooling rate and metal thickness, *Material Science and Eng*ineering, **A278**, 2000, pp. 142-150 (doi:10.1016/S0921-5093(99)00581-X).

[2] V.K. Tolpygo and D.R. Clarke. Spalling failure of α-alumina films grown by oxidation. II. Decohesion nucleation and growth, *Material Science and Eng*ineering, **A278,** 2000, pp. 151-161 (doi:10.1016/S0921-5093(99)00582-1).

[3] S. Wang, C.M. Harvey and B. Wang, Room temperature spallation of α-alumina films grown by oxidation, *Engineering Fracture Mechanics*, available online 14th March 2017 (doi: 10.1016/j.engfracmech.2017.03.002).

[4] C.M. Harvey, B. Wang and S. Wang, Spallation of thin films driven by pockets of energy concentration, *Theoretical and Applied Fracture Mechanics,* available on line 21st April 2017 (doi: 10.1016/j.tafmec.2017.04.011).

[5] S. Wang S and C.M. Harvey, A theory of one-dimensional fracture. *Composite Structures*, **94**, 2012, pp.758–767 (doi: 10.1016/j.compstruct.2011.09.011). Also a plenary lecture at the 16th International Conference on Composite Structures (ICCS16), 28–30 June 2011, Porto, Portugal.

[6] S. Wang and C.M. Harvey, Mixed mode partition theories for one dimensional fracture, *Engineering Fracture Mechanics*, **79**, 2012, pp. 329-352 (doi: 10.1016/j.engfracmech.2011.11.013).

[7] C.M. Harvey and S. Wang, Mixed mode partition theories for one dimensional delamination in laminated composite beams, *Engineering Fracture Mechanics*, **96**, 2012, pp. 737-759 (doi: 10.1016/j.engfracmech.2012.10.001).

[8] C.M. Harvey and S. Wang, Experimental assessment of mixed-mode partition theories, *Composite Structures*, **94**, 2012, pp. 2057-2067 (doi: 10.1016/j.compstruct.2012.02.007).

[9] C.M. Harvey, M.R. Eplett and S. Wang, Experimental assessment of mixed-mode partition theories for generally laminated composite beams, *Composite Structures*, **124**, 2015, pp. 10-18 (doi: 10.1016/j.compstruct.2014.12.064).

[10] J.W. Hutchinson and Z. Suo, Mixed mode cracking in layered materials, *Advances in Applied Mechanics*, **29**, 1992, pp. 63-191 (doi:10.1016/S0065-2156(08)70164-9).

[11] C.M. Harvey, J.D. Wood, S. Wang and A. Watson, A novel method for the partition of mixed-mode fractures in 2D elastic laminated unidirectional composite beams, *Composite Structures* **116**, 2014, pp. 589-594 (doi: 10.1016/j.compstruct.2014.05.041).